CHAPTER 2

Rational Design of Mixed Nanoclusters: Metal Shells Supported and Shaped by Molecular Cores

FEDOR Y. NAUMKIN

Faculty of Science, UOIT, Oshawa, ON L1H 7K4, Canada

2.1 Introduction

Atomic and molecular clusters are the central objects of studies explosively expanding in recent decades due to the ever-increasing capability to produce and manipulate them. These nanometer-sized systems are, by definition, at the very heart of modern nanoscience and nanotechnology, and, due to their endless variety, have every chance of staying there in future. Scaling the size of a cluster of a given composition between the limits of a single atom/molecule and the corresponding bulk material implies variation of properties between those (very different) of a quantum and a classical entity. In particular, metal clusters can exhibit semiconductor or insulator properties;[1,2] gold, famous for chemical inertness in bulk quantities, becomes a versatile and efficient catalyst at cluster scale;[3] small metal clusters (''superhalogens'') show electron affinities exceeding that of halogen atoms,[4] *etc*.

Cluster composition is another parameter strongly affecting cluster properties. For atoms or molecules of two different pure substances, A and B, the mixed cluster A_mB_{n-m} of a fixed size n can apparently cover the whole interval

RSC Theoretical and Computational Chemistry Series No. 4
Computational Nanoscience
Edited by Elena Bichoutskaia

Published by the Royal Society of Chemistry, www.rsc.org

of properties between those of A_n and B_n with varying m. Further degrees of freedom are associated with more-than-binary systems. This is reflected by the quickly developing research in the area of doped (with both a nonmetal dopant atom in a metal host and *vice versa*)[5–7] and mixed (with multiple dopant atoms) clusters such as metcars[8] and nanoalloys (with dopant and host as different metals).[9]

Yet another factor is the cluster shape, which can considerably alter properties between different isomers of otherwise the same (in terms of size and composition) system. One relevant example of a system currently defining a whole new research area is graphene, an all-flat isomeric form of carbon (with a honecomb-shaped one-atom thick grid of atoms). Here, we could certainly recall other famous isomers of carbon like diamond, fullerenes, and carbon nanotubes, all with very different properties. By analogy with carbon species, metal cluster cages and nanotubes *versus* bulk crystalline solid are appropriate examples as well.[10,11]

An enormous multitude of property designs is accessible by combining the above factors, such as shape and size variations of clusters of mixed composition, for instance as in gold-covered fullerenes[12] and layered ''onion'' clusters.[13] Sometimes, one factor can spontaneously involve another. For instance, gold clusters switch from energetically preferred 2D to 3D geometry with increasing size (see, *e.g.*, ref. 14); doping a pure cluster with a different atom can induce shape change, such as originally planar (rhombic) metal tetra-atom (Al_4, Au_4) forming with the added carbon or silicon atom a tetrahedral methane-like structure[15–17] due to the dopant's inherent bond pattern, *etc.*

An extra dimension can be added when considering shape changes enabled by ''dopants'' forming no covalent bonds to the host cluster. For instance, water molecules are known to form hydrogen-bonded cages around inserted hydrophobic molecules such as saturated organics (methane, *etc.*). By analogy, we could imagine a metal cage (shell) surrounding a closed-shell atom or molecule (core) suspended inside it electrostatically, say *via* weak van der Waals or maybe (if a core–shell charge transfer occurs) appreciable Coulomb interaction. In particular, such an arrangement would facilitate exploring the otherwise inaccessible shape-related properties of a cage that would collapse without such a supporting ''filler'' inside. Moreover, using molecular cores of appropriate sizes and geometries, we could attempt designing metal-shell based nanosystems with desirable shapes and related properties. One recent example of a relevant system created experimentally is gold-covered polymer nanorods.[18]

In this work, we present and review recent studies of core–shell clusters with nonmetal atomic and molecular centres (C_n, CH_4, H_2) encapsulated into metal cluster shells (Au_n, Al_n, Mg_n). Both open- and closed-shell cores, bonded to the shell covalently (C_n) and electrostatically (CH_4, H_2), as well as the shells both stable by themselves as cages (with no core inside) and not stable are considered. The focus is on structures and stabilities, while charge distributions and some other electronic properties (excitation and ionisation energies, electron affinity) are also discussed.

2.2 General Aspects of Computational Procedure

All calculations have been carried out using the NWChem computational chemistry package,[19] and obtained structures visualised with the ViewMol3D molecular modelling software.[20] For relatively small C_nM_m ($n = 1$–3, $m = 1$–8, M = Au, Al) species an MP2 level of theory has been preferred, replaced due to the size of the system by DFT(B3LYP) for larger C_nAu_m ($n = 5$ and 10, $m = 12$ to 24) systems. The MP2 theory has also been used for $H_2@Mg_n$, while both approaches employed for $H_2@Au_{12}$ and $CH_4@Au_{12}$. These standard methods are implemented in NWChem.

Basis sets for atoms have varied from 6-31G* for carbon and hydrogen in larger C_nAu_m, $H_2@Au_{12}$ and $CH_4@Au_{12}$, to aug-cc-pVTZ for all atoms in small C_nAu_m, C_nAl_m and $H_2@Mg_n$. For gold, a standard choice has been the LANL2dz effective core potential (ECP) and associate basis set, with limited corrections using the Stuttgart's RSC (relativistic small-core) ECP and basis set. Details of all these bases are available at the PNL's Basis Set Exchange online facility.[21] In particular, the results for identical basis sets and methods used for larger C_nAu_m, $CH_4@Au_{12}$, and $H_2@Au_{12}$ allow a direct quantitative comparison of these systems. The choice of methods and basis sets is governed by a reasonable compromise between the accuracy judged from comparison to available experimental data or highly reliable calculated results for small fragments (such as ionisation energies and electron affinities for atoms, dissociation energies and equilibrium distances for diatoms),[22] and the acceptable time of calculations.

All-atom symmetry-unconstrained optimisation has been employed, and energy minima verified in terms of all-real vibrational frequencies. For each species, energies for both lowest and higher spin states are calculated, in order to properly establish the ground state multiplicity. For every system, multiple initial geometries have been tried. For the C_nAu_m and C_nAl_m species, it appears reasonable to start, in particular, with structures of metal-substituted C_nH_m molecules. The rationale behind this is the relations between the relative bond strengths (C–C > C–M > M–M), so that the integrity of carbon skeletons is preserved, while efficient carbon–metal interaction is enabled in the hydrocarbon-like structures. Hence, it is anticipated that such a starting point should lead to low-energy isomers. Besides, this allows considering species likely to be produced in experiments effectively *via* such a metal substitution, so that optimisation could mimic a subsequent process leading to realistic products. For the $H_2@Au_{12}$ and $CH_4@Au_{12}$ systems, a few possible orientations of a molecule inside a metal cluster cage, as well as a few different cage structures, are attempted.

It is possible that the resulting optimised geometries correspond to local energy minima. Finding the global minimum, *i.e.* lowest-energy isomer, is certainly important and desirable, while it is realised that identifying higher-energy isomers is also significant, especially if they may be stabilised by high enough energy barriers to be sufficiently long-living for practical purposes. An apparent support of their role, directly relevant to this work, is a variety of the

isomers of virtually each hydrocarbon molecule, readily produced in experiments and having various useful applications. Thus, for instance, we should not aim only at graphite while suspecting possibility of diamond. One recent example related to the present work is the structure of the $SiAu_{16}$ cluster, predicted to have a higher-energy symmetric core–shell isomer $Si@Au_{16}$,[23] as well as a lower-energy isomer with Si attached to the surface of asymmetric Au_{16}.[24]

Another, related aspect is that the lower-energy species are usually easier to obtain experimentally, at least with currently established procedures. However, experimental methods develop quickly. Furthermore, if a higher-energy isomer promises (at least theoretically) to possess very attractive properties, then stronger efforts to find new, unusual ways to efficiently produce it will be fully justified, very likely made, and probably succeed. A recent illustration may be the experiments on generating carbon–gold clusters by laser vaporisation of gold-covered carbon rods,[25] producing carbon-dominated products with only a few (mainly one) gold atoms. One could interpret this outcome as a likely consequence of the target structure, with the gold layer evaporated first and being almost gone by the time carbon begins to vaporise. One possible attempt to overcome this could be to try also to invert the situation and enrich clusters with gold *via* irradiating carbon (graphite?) -covered gold targets. At least, the above considerations regarding relative bond strengths and their reflection in the stable system structure are consistent with these experimental results.

2.3 Results and Discussion

The presentation of results is organised as follows. First, systems with cores forming bonds to shell atoms are considered, in the general order of increasing size, beginning with the core. Secondly, saturated closed-shell cores non-covalently suspended inside the shell are introduced.

Hence, starting from a single carbon atom with a few gold atoms attached, we proceed to a carbon diatomic core, then look at the differences associated with replacing Au by Al atoms, and the core is then increased to a triatomic molecule. The next step involves return to auro-carbon systems, with the gold shell surrounding the carbon core represented by penta and deca-atomic (radical) species. In the following stage, the core is changed qualitatively, to a small hydrocarbon molecule (methane) as a closed-shell counterpart of the C_5 radical. Finally, the core is reduced to a very small (hydrogen) diatom, and then evolves into a hydrogen dimer, both encapsulated in cluster cages of magnesium atoms. The last case thus deals with more than one molecule inside a metal shell.

2.3.1 Small Gold Clusters Doped by Carbon

2.3.1.1 CAu_n ($n = 2$-6)

Adding a carbon atom to the gold diatom along or perpendicular to its axis produces two isomers, linear CAuAu and isosceles-triangular counterpart of

methylene, respectively (Figure 2.1), similar to the $SiAu_2$ counterpart.[17] Gold clusters of three to several atoms are known to prefer planar structures composed of near-equilateral triangular Au_3 units fused by their sides (for example, Au_4 is a rhombus).[14] Accordingly, the C atom can be attached to the corner, side, or face of Au_3, producing planar Y-shaped and cyclic, and near-planar methyl-like isomers, respectively.

For both CAu_2 and CAu_3, the relative stability of isomers appears to be simply related to the number of stronger C–Au bonds, so that the energy for complete dissociation (into atoms) increases from linear (one bond) to triangular (two) CAu_2 and from corner- (one bond) to side- (two) to face-bound (three) CAu_3. In particular, for analogous $SiAu_3$, methyl-like isomer has also been found to be most stable.[17] The same trend is preserved for CAu_4, the tetrahedral (T_d) methane-like isomer being most stable, similar to $SiAu_4$,[17] followed by asymmetric trigonal bipyramidal (ATB), planar B-shaped and Φ-shaped, with four to one C–Au bonds, respectively, the first two isomers being identified previously as well.[16]

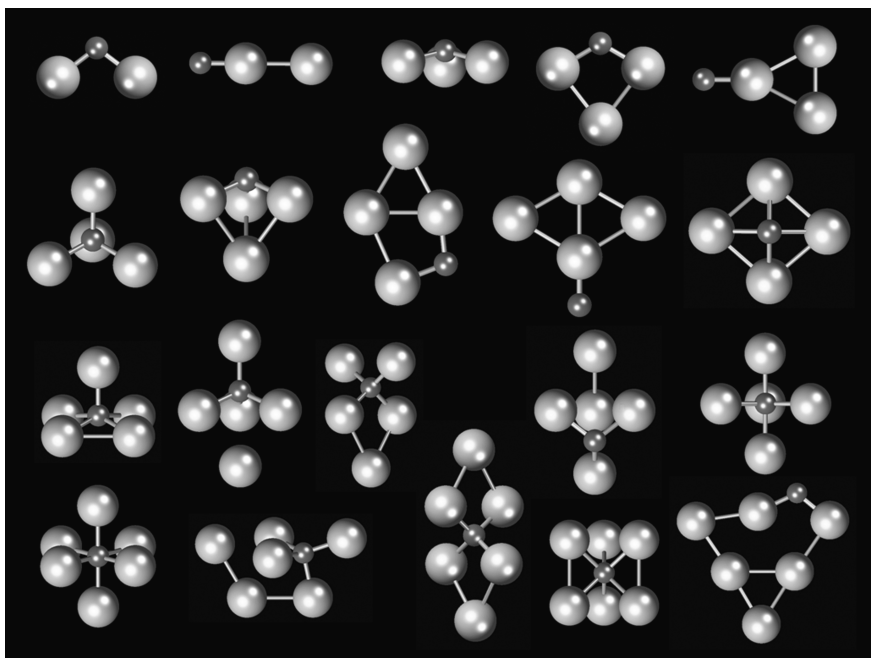

Figure 2.1 Optimised geometries of: the bent and linear isomers of CAu_2 (top row left), and the methyl-like, cyclic and Y-shaped isomers of CAu_3 (right); the methane-like, trigonal-bipyramidal, planar B- and Φ-shaped isomers, and transition state of CAu_4 (2nd row); the square-pyramidal, trigonal-bipyramidal, γ-shaped, and capped-ATB isomers, and transition state of CAu_5 (3rd row); the octahedral, capped-ATB, twisted-8-shaped, trigonal-prismatic, and planar isomers of CAu_6 (bottom row).

Starting from $n = 4$, adding the C atom transforms planar Au_n into 3D shells around the carbon core, at least for the most stable isomers of CAu_n (like the T_d isomer of CAu_4). Their higher-energy isomers can be obtained by attaching another Au atom to gold atoms of CAu_{n-1} (like the ATB isomer of CAu_4, with 4th Au attached to the Au_3 face of CAu_3) or C atom to Au_n (like the B- and Φ-isomers of CAu_4), see Figure 2.1. It is worth noting that adding C to the other corner of the Au_4 rhombus still leads to the Φ-isomer, thus effectively "rotating" the gold component.

The CAu_4 structure with C attached centrally to (bent) rhombic Au_4, predicted previously (with DFT) as an isomer,[16] is found (with MP2) to be a transition state relaxing to the T_d isomer, apparently due to an unfavourable C–Au bond pattern. However, the CAu_5 isomer predicted to be most stable in this work can be viewed as such a CAu_4 structure stabilised by attaching 5th Au to the carbon atom, on the opposite side (Figure 2.1). The resulting square-pyramidal CAu_5 species, analogous to that predicted for $SiAu_5$,[26] represents an unusual case of pentacoordinated carbon, also different from normally expected trigonal bipyramidal structure for such a coordination, as, *e.g.* for the CLi_5 counterpart.[27] In fact, the latter structure for CAu_5 is predicted to be a transition state relaxing to the square pyramid.

Three other isomers, in the order of increasing energy, can be obtained by attaching a 5th Au to the Au_3 face (adding three new Au–Au pair interactions in the resulting asymmetric trigonal bipyramid) or to the Au_2 side (two such interactions in the resulting γ-shaped isomer) of the T_d isomer of CAu_4, and to the Au_3 face of the (higher-energy) ATB isomer of CAu_4. Again, the relative stability of the CAu_5 isomers follows the number of C–Au bonds – from five to three. Starting from CAu_5, the similarity of at least some isomers to corresponding hydrocarbons is lost, as expected.

The most stable isomer of CAu_6 found in this work is octahedral, with hexacoordinated carbon atom at its centre (Figure 2.1), obtained by relaxing the above CAu_5 square pyramid with a 6th Au attached centrally to its base. This geometry is what is normally expected for such a coordination (found also, *e.g.*, for CLi_6 [27]) which, however, is still rather unusual for carbon.

Two higher-energy isomers correspond to 6th Au attached to the Au_3 face (farther from C) of the above (higher-energy) ATB, and to the Au_2 side (opposite the 5th Au added before) of γ-shaped CAu_5, resulting in a twisted-8-shaped isomer of CAu_6. An isomer with a still higher energy is another unusual species with hexacoordinated carbon at the centre of a trigonal prism of the gold shell, produced *via* relaxing either the ATB or the square-pyramidal isomer of CAu_5 with 6th Au attached to its Au_3 face. The least-stable isomer of those studied here is obtained by attaching C atom to a side of the planar (near-equilateral triangular) Au_6. Here, the general trend of stability decreasing with the number of C–Au bonds (from six to four to two for the above isomers) is violated by the trigonal-prismatic isomer, indicating a higher strain for its bond pattern, with the AuCAu bond angles of less than 85°.

The above isomers of CAu_2 and CAu_3 are separated by energy differences of about 2 eV. For CAu_4 the gap between the lowest-energy and nearest next

Table 2.1 Characteristic energies (in eV) of the lowest-energy isomers of CAu_n.

n	D_e ($\rightarrow C + n\,Au$)	D_e ($\rightarrow CAu_{n-1} + Au$)	D_e ($\rightarrow C + Au_n$)	VE^{*a}	VIE	VEA
2	6.63	3.57	4.74	0.75	8.51	0.89
3	10.0	3.37	7.07	2.59	7.46	2.64
4	14.0	3.99	8.56	2.48	8.31	1.08
5	15.5	1.50	7.95	2.84	5.95	2.46
6	17.9	2.42	7.18	1.34	6.51	0.87

[a] $S = 0 \rightarrow 1$ for even n, $S = 1/2 \rightarrow 3/2$ for odd n

isomer reduces to ≈ 1 eV, which recovers to $\approx 2 \pm 0.5$ eV for the subsequent isomers. For CAu_5 and CAu_6, however, respectively two and three higher energy isomers are within 0.3 ± 0.05 eV of the lowest-energy isomer.

The equilibrium distance R_e(C–Au) for the lowest-energy isomers found in this work steadily increases from CAu to CAu_6, slowly up to $n = 4$ and then faster for $n = 5, 6$. The overall variation falls within 15%, and the bond lengths are about 2 Å. In the lowest-energy CAu_4 and CAu_6 all R_e(C–Au) are equal, and in the square-pyramidal CAu_5, the axial C–Au bond is slightly shorter (by ≈ 0.1 Å) than the other four. The R_e(Au–Au) distance is longest in CAu_3, only slightly shorter in CAu_4, and in CAu_6 recovers the value for CAu_2, varying within 7%. In all systems, R_e(Au–Au) of about 3 Å is significantly longer than in isolated Au_2 (2.5 Å), consistent with dominant C–Au bonding.

For the lowest-energy isomers, the total dissociation energies $D_e(CAu_n \rightarrow C + n\,Au)$ per atom vary relatively weakly with n, peaking for $n = 4$ (Table 2.1). The energies $D_e(CAu_n \rightarrow CAu_{n-1} + Au)$ for detachment of one Au atom from CAu_n show a slow increase of up to $n = 4$, and then a sharp drop for the hypercoordinated carbon case with $n = 5$, followed by a significant increase for $n = 6$. The highest relative stability of the methane-like CAu_4 is further confirmed by the energies $D_e(CAu_n \rightarrow C + Au_n)$ for removal of the C atom, with their faster increase with n before, and a slower decrease after $n = 4$. In both cases the remaining CAu_{n-1} and Au_n are reoptimised. Thus, from CAu to CAu_4 the stabilisation of the system with adding Au atoms accelerates with increasing n due to more binding contributions: with each Au, one C–Au bond plus $n - 1$ Au–Au interactions are added. In CAu_4 the valence of carbon is saturated, and the system has a total of "magic" 8 valence electrons in its atoms. In CAu_5 and CAu_6, the C–Au bonds are strained due to the hypercoordination of carbon and the gold shell is overcrowded with atoms, slowing down the further stabilisation.

We can approximately partition the total dissociation energy $D_e(CAu_n \rightarrow C + n\,Au)$ using a simple model of effective D(C–Au) and D(Au–Au) pair components. Then, for CAu_4:

$$D_e(CAu_4) \approx 4D(C - Au) + 6\,D(Au - Au).$$

Similarly, for the CAu_3^* fragment with atoms frozen in the same positions as in CAu_4:

$$D_e(CAu_3{}^*) \approx 3\,D(C - Au) + 3\,D(Au - Au).$$

Using $D_e(CAu_4)$ and $D_e(CAu_3^*)$ calculated at the same level of theory and solving the above two equations, we obtain D(C–Au) $\approx$2.8 eV and D(Au–Au) $\approx$0.5 eV. These sum up to $\approx$11 eV of total carbon-gold and $\approx$3 eV of total gold–gold interaction in CAu_4. The net aurophilic interaction in this case thus contributes $\approx$21% to the total binding.

From similar calculations for octahedral CAu_6 and its (frozen) CAu_5^* fragment, D(C–Au) $\approx$2.6 eV and D(Au–Au) $\approx$0.2 eV, adding up to 6 D(C–Au) $\approx$16 and 12 D(Au–Au) $\approx$2.2 eV for the total carbon–gold and gold–gold interactions, respectively. The latter value is considerably less relative to that for CAu_4, even though the number of the Au–Au pair interactions is doubled. This leads to $\approx$12% of binding due to aurophilic interaction, about half of the value for CAu_4. Such a reduction can be explained in terms of shorter Au–Au distances and therefore stronger repulsion of the positively charged Au atoms in CAu_6, weakening the net aurophilic interaction. The partial charge on the atoms is implicitly accounted for in their effective interactions.

For the lowest-energy isomers of CAu_n, the negative charge on carbon increases with the number of Au "electron donors", almost linearly up to $n=4$, then significantly (about twice) more slowly for $n=5$ and 6, reflecting a reduced ability of the carbon anion to accept more electrons. As a result, the C atom carries $\approx$–2e in CAu_4, and even more in the hypercoordinated species. Availability of at least two extra electrons could enable formation of extra bonds, such as one and two additional C–Au bonds in CAu_5 and CAu_6, respectively. The charges on gold atoms increase with n slightly, leveling at $\approx$0.5e already for $n=3$. Using these charges and the equilibrium Au–Au distances, a simple sum of Coulomb Au–Au pair repulsions in CAu_6 is about twice that in CAu_4, consistent with the above considerations for the total gold–gold interactions in these systems.

The lowest-energy isomers of CAu_n have moderate ($\approx$1 D for $n=2$, 3), small ($\approx$0.2 D for $n=5$), or no dipole moments (for $n=4$, 6). Calculated critical electron densities in these isomers are equal (or nearly equal in CAu_5) for all C–Au bonds, and slowly decrease with increasing n. Their values for $n=2$ to 4 are about half those for the C–H bonds in the corresponding CH_n molecules.

For the lowest-energy isomers of CAu_n, each of vertical spin-excitation energy VE* (effectively the HOMO–LUMO gap), ionisation energy VIE and electron affinity VEA show typical even-odd oscillations in values with increasing cluster size, reflecting spin-pairing for even n (Table 2.1). The VIE values generally decrease with increasing n, while VE* appear to slowly increase and VEA to remain about constant on average, at least in the studied size range.

The CAu_5 cluster offers an interesting example of property evolution with geometry variation and "doping" a small gold cluster by a carbon atom. When the (lowest-energy) planar isomer of Au_5 is transformed into the higher-energy trigonal-pyramidal one, its VE* value drops dramatically, but is then recovered on adding the C atom to its surface (at the Au_3 face). The further transitions to the ATB isomer (with C "sinking" into the cluster) and then to the square-pyramidal isomer do not, however, noticeably affect the VE* value (Table 2.2). At the same time, the VIE and VEA values vary weakly (within 10–15%) with

Table 2.2 Characteristic energies (in eV) of Au_5 and CAu_5 isomers.

System	D_e[a]	*VE*(S = 1/2→3/2)*	*VIE*	*VEA*
Au_5 (planar)	7.54	2.56	6.77	2.60
Au_5 (trigonal bipyr.)	6.90	0.65	6.47	2.23
CAu_5 (capped ATB)	13.9	2.65	6.00	2.31
CAu_5 (ATB)	15.3	2.76	6.05	2.52
CAu_5 (square pyr.)	15.5	2.84	5.95	2.46

[a] $Au_5 \rightarrow 5\,Au$, $CAu_5 \rightarrow C + 5\,Au$

either the shape change or the ''doping'', the former decreasing and the latter going through a shallow minimum at the 2D to 3D transition in Au_5 and then recovering. Both these alterations are counterintuitive in terms of higher IE and lower EA of C relative to Au.

The open-shell CAu_5 system could be expected to be a reactive species with a low chance of sufficiently long survival in experiments. It turns out that its dimer, $(CAu_5)_2$ can preserve the unique pentacoordination of both carbon atoms while being a stable closed-shell system, consistent with its ''magic'' total number (18) of valence electrons in atoms. Accordingly, the electron affinity drops dramatically from the monomer to the dimer, from VEA $\approx$2.5 to $\approx$0.6 eV. The corresponding variations of VIE and VE* are relatively weaker, the former value increasing and the latter decreasing by $\approx$25%. The system can be obtained by joining two CAu_5 units by their square bases in a staggered geometry (Figure 2.2). The binding energy of the monomers is $\approx$4.5 eV, and similar to the monomer case, the dimer structure is destabilised by detachment of an axial Au atom.

The above CAu_n ($n > 3$) species can be formally treated as core–shell systems with a single-atom carbon centre surrounded by a one-atom thick layer of gold. Next, we will increase the core size to two atoms.

2.3.1.2 C_2Au_n (n = 1–6)

From the above analysis of the CAu_n species it appears that the most stable isomers of auro-carbons could be expected to resemble hydrocarbons for up to

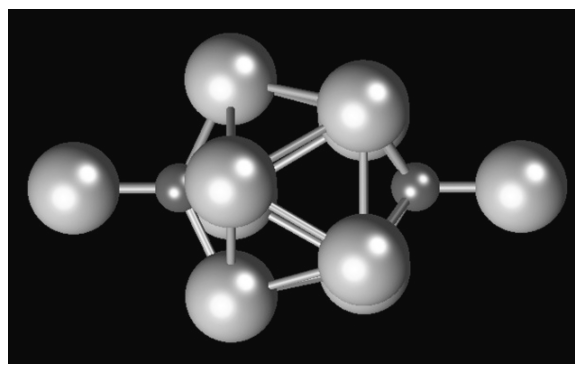

Figure 2.2 Optimised geometry of the $(CAu_5)_2$ dimer.

formal saturation of valence in the C atom, and, for more gold in the system, to have structures possibly different from those of saturated-carbon species with extra Au atoms attached. In this section we check this assumption for some analogous dicarbon-core systems.

The C_2Au and C_2Au_2 systems are linear, similar to the CCH (ethynyl) radical and the acetylene molecule, respectively (Figure 2.3), in accordance with the earlier work.[28] The T-shaped $CCAu_2$ structure (with C_2 perpendicular to Au_2) is a transition state, unlike the stable CCH_2 (vinylidene) radical, likely due to a significant repulsion of large and charged gold atoms close to one another in such a geometry. Such a repulsion is minimised in the linear AuCCAu geometry.

The C_2Au_3 species is T-shaped, with 3rd gold atom attached sideways to the middle of the above AuCCAu system (Figure 2.3), which is different from the

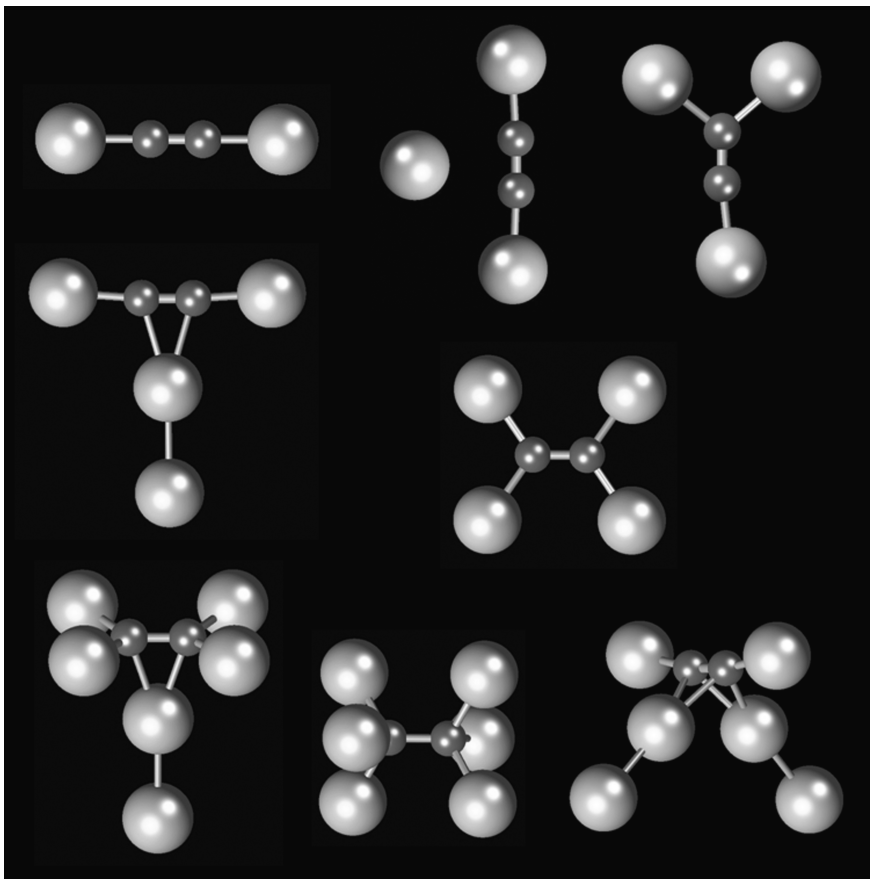

Figure 2.3 Optimised geometries of: C_2Au_2, the T-shaped and vinyl-like isomers of C_2Au_3 (top row); the T-shaped and ethylene-like isomers of C_2Au_4 (middle row); the T-shaped, ethane-like, and right-angled isomers of C_2Au_6 (bottom row).

H_2CCH (vinyl) radical. In fact, the vinyl-like Au_2CCAu structure corresponds to another isomer only ≈ 0.2 eV higher in energy.

Addition of the 4th Au atom can lead to two gold atoms on each end of C_2 in ethylene-like Au_2CCAu_2 isomer (Figure 2.3) identified earlier as well.[28] A rhombic structure with the 4th Au atom attached to dicarbon opposite the 3rd one in CAu_3, which could be expected instead, is a transition state separating equivalent ethylene-like isomers. The slightly (by ≈ 0.3 eV) more stable, lowest-energy isomer of C_2Au_4 predicted in the present work is T-shaped, with the gold dimer attached perpendicular to AuCCAu at its middle. Its higher stability is consistent with the above result for C_2Au_3. It is interesting to note a geometric similarity of this structure to that of the weakly bound C_2H_2–H_2 complex.[29] So there appears to be an inversion of the relative stability of the ethylene and T-shaped geometries for the auro-carbon and hydrocarbon counterparts.

For C_2Au_6, two predicted isomers evolve from the above two isomers of C_2Au_4. One, right-angled, has a 2nd gold dimer attached perpendicular the AuCCAu unit at its middle, at an angle of about 90° to the 1st gold dimer (Figure 2.3). There is a transition state separating equivalent such structures, with the 2nd dimer at 180° to the 1st one in a planar cross-shaped geometry. Another isomer, also identified previously,[28] is ethane-like, with two bonded CAu_3 groups in a staggered arrangement. Here, a transition state is similar to that of C_2H_6, with two such groups in the aligned arrangement, *i.e.* with one group rotated about the axis by 30°. The third, most-stable isomer of C_2Au_6 is found to be T-shaped, an alternative extension of T-shaped C_2Au_4, with a single gold dimer attached perpendicular to ethylene-like C_2Au_4 at its middle. These three isomers of C_2Au_6 are within 0.15 eV of one another in energy.

From C_2Au_2 to ethylene-like C_2Au_4, and then to ethane-like C_2Au_6, the equilibrium R_e(C–C) and R_e(C–Au) distances increase from 1.25 Å and ≈ 1.9 Å by ≈ 0.1 Å and ≈ 0.05 Å, respectively, consistent with their variation in the hydrocarbon analogues. Attachment to C_2Au_2 of a gold atom in C_2Au_3 or dimers in T-shaped C_2Au_4 and C_2Au_6 increases R_e(C–C) by ≈ 0.01 Å per atom or ≈ 0.02 Å per dimer, attachment of Au_2 to C_2Au_4 in C_2Au_6 inducing double the latter stretch. The distance between each atom of the C_2 core and the nearest gold atom attached to its middle drops from ≈ 2.5 Å in C_2Au_3 (single Au atom) by ≈ 0.3 Å in the systems with attached Au_2, the dimers remaining almost unperturbed as compared to an isolated gold diatom.

For the lowest-energy isomers the dissociation energies $D_e(C_2Au_n \rightarrow C_2 + n\,Au)$ decrease from ≈ 3.5 to ≈ 2.5 to ≈ 2.3 eV per Au atom for $n = 2$ to 4 to 6, respectively. The last two values are significantly smaller than 3.4 ± 0.1 eV for CAu_n ($n = 2$–4) due to relaxation of C_2. Detachment of Au from the AuCCAu unit in C_2Au_3 requires ≈ 0.6 eV of energy. The value considerably increases, to ≈ 1.5 eV, for detachment of the gold dimer in T-shaped C_2Au_4, and further to ≈ 1.7 eV for the 2nd such dimer in right-angled C_2Au_6. In T-shaped C_2Au_6 the dimer is attached to the Au_2CCAu_2 unit by ≈ 1.8 eV.

The above results allow us to conclude that structural analogues of C_2H_n are likely to be at least low-energy isomers of C_2Au_n. However, the auro-carbon lowest-energy isomers can resemble higher-energy, weakly bound hydrocarbon

systems still preserving the (unsaturated) hydrocarbon-like unit in their structure but with gold dimers attached perpendicular to its middle. In particular, we could anticipate similar stable structures of larger C_2Au_n, *e.g.* with three, four and perhaps more gold dimers around the AuCCAu unit (for $n = 8$, 10, *etc.*), and possibly with at least two dimers on the opposite sides of the Au_2CCAu_2 unit (for $n = 8$), the relevant further work being in progress. The dicarbon core can thus be surrounded by a gold shell composed of atomic and diatomic units.

To this point, small core–shell auro-carbon systems have been studied, with up to a dicarbon core. In the following section, we will consider similar alumo-carbon species,[30] to compare with another metal component of a different valence.

2.3.2 Small Alumo-Carbon Clusters

2.3.2.1 C_2Al_n ($n = 2$–6)

The most stable CAl_n isomers have been found previously[15,31] to be similar to those of respective CAu_n for $n = 3$ and 4, except for planar CAl_3 as compared to near-planar CAu_3. A higher-energy isomer of CAl_4 has been predicted to be planar,[15] in qualitative agreement with the above results for CAu_4.

Similar to C_2Au_n, the most stable isomers are acetylene-like AlCCAl for $n = 2$, with another Al atom attached to its middle for $n = 3$, thus confirming previously identified geometries.[32,33] Unlike for the corresponding auro-carbons, however, C_2Al is T-shaped (isosceles-triangular), the linear CCAl system being ≈ 1 eV higher in energy, and there is a ≈ 2 eV higher-energy T-shaped isomer of C_2Al_2, with the aluminium dimer attached perpendicular to C_2 at its middle.

The lowest-energy isomer of C_2Al_4 is found to be rhombic, with two Al atoms attached on the opposite sides of AlCCAl (Figure 2.4), which structure represents a transition state for C_2Au_4. Interaction of dicarbon with the originally rhombic Al_4 thus stretches the aluminium cluster symmetrically into a frame around the carbon core. No ethylene-like isomer is found for this system, unlike for C_2Au_4. In fact, the ethylene-like structure relaxes to a ≈ 1 eV higher-energy nonplanar isomer of C_2Al_4, structurally resembling C_2Al_3 but with two Al atoms added on the same side of AlCCAl and forming a dimer at one end of C. An interesting feature of the rhombic isomer is two planar-tetracoordinated carbon atoms with nonperpendicular C–Al bonds.

Adding two Al atoms at the same or opposite sides of C_2 in C_2Al_4 results in a "side-on" isomer of C_2Al_6, with the Al_2 dimer attached sideways to the still flat but distorted C_2Al_4 base, thus creating an aluminium shell half-enclosing the dicarbon core (Figure 2.4). It is interesting to note that the shell does enclose C_2 completely, by forming a square "belt" around the waist of AlCCAl in the anionic derivative of C_2Al_6. Upon electron detachment from $C_2Al_6^-$, the resulting neutral system recovers its geometry with the dicarbon half-exposed. We could anticipate that adding another aluminium dimer on the exposed side of C_2 could complete the aluminium shell around the carbon core in C_2Al_8.

Isolated Al_6 cluster is a skewed rectangle bipyramid, which geometry would formally match the ethylene-like C_2Al_6 structure with C_2 inside, by analogy

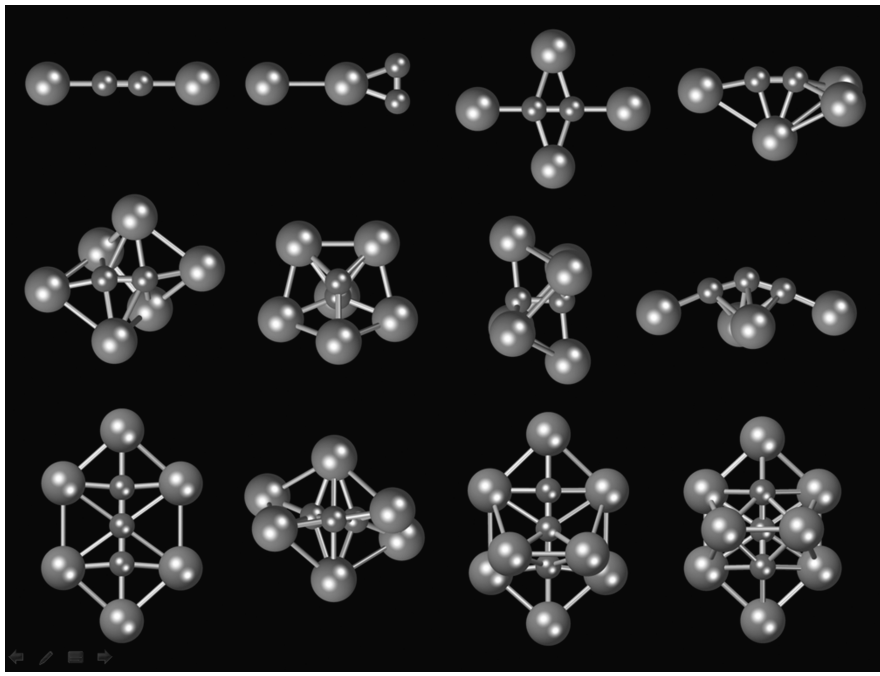

Figure 2.4 Optimised geometries of: the linear and T-shaped isomers of C_2Al_2, planar and nonplanar isomers of C_2Al_4 (top row), the side-on and end-on isomers of C_2Al_6, ethane-like transition state between equivalent end-on isomers, and C_3Al_4 (middle row); the planar and nonplanar (with a C_3-cycle core) isomers of C_3Al_6, and skewed and symmetric isomers of C_3Al_8 (bottom row).

with C_2Al_4. Such a geometry is, however, found to be a transition state between equivalent "end-on" isomers ≈ 0.5 eV lower in energy than the "side-on" one, with the dicarbon protruding from an aluminium "cup". So, this is another example of isomers of auro-carbons correlating to transition states of corresponding alumo-carbons and *vice versa* (as, *e.g.*, for C_2Al_4 and C_2Au_4 above).

We can conclude that while small CAl_n ($n = 2$ to 4) species are structurally similar to respective CAu_n, the C_2Al_n and C_2Au_n systems (except for $n = 2$, 3) have quite different isomers. This could be related to the extra valence electrons in Al as compared to Au, enabling more efficient Al–Al bonding, which possibility is reduced in the C_2Au_n species dominated by C–Au bonding.

For the lowest-energy isomers predicted here, the dissociation energies $D_e(C_2Al_n \rightarrow C_2 + n\ Al)$ per atom drop from 5 eV for $n = 2$ to ≈ 4 eV for $n = 4$ and 6, reflecting a weaker binding of aluminium atoms on the sides of dicarbon as compared to along its axis. The energy $D_e(C_2Al_n \rightarrow C_2 + Al_n)$ for removal of C_2 from the (relaxing) Al_n frame slightly increases with n, being around 9 eV. For the systems with even number of Al atoms, relative stabilities can be conveniently discussed also using dissociation energies $D_e(C_2Al_n \rightarrow C_2Al_{n-2} + Al_2)$. Detachment of an aluminium dimer from C_2Al_2, C_2Al_4 and C_2Al_6 requires ≈ 9, ≈ 4 and ≈ 6 eV, respectively. The lowest relative stability of

C_2Al_4 with its total of 20 valence electrons in atoms suggests that in systems of atoms with very different electronegativities, such as carbon and aluminium, "magic" numbers of electrons may be unreliable indicators. This is further supported by the highest (also among all system studied) VEA ≈ 1.7 eV and the lowest VE* and VIE of C_2Al_n for $n = 4$. The C_2Al_6 system exhibits the highest VE* ≈ 3.5 eV and VIE ≈ 9.5 eV among all C_nAl_m studied.

The equilibrium distance R_e(C–C) in C_2Al_n steadily increases from 1.25 Å in C_2Al_2 by ≈ 0.1 Å per each additional Al_2, in accordance with more metal atoms donating electrons and thus weakening the C–C bonding. The R_e(C–Al) distances are about same, ≈ 2 Å, for the Al atoms attached axially to C_2, and significantly longer (by ≈ 0.1–0.3 Å) for the atoms attached to its sides.

The charge on the carbon core is -1.5e in C_2Al_2, double that in C_2Al_4, then increases (in absolute value) more weakly in C_2Al_6. The value of the charge on each C atom reaches ≈ -2e, potentially enabling extra bonds for the hypercoordinated atoms. However, for the carbon formal pentacoordination in the "side-on" isomer and even heptacoordination in the "end-on" isomer of C_2Al_6, no hypervalence is found in terms of the critical points of electron densities (within the atoms-in-molecules, AIM, formalism[34]), the C atoms being tetrabonded. The electron-density distributions indicate a weakly covalent C–Al bonding (with appreciable electron density between atoms) for the axial aluminium atoms and ionic bonding for those on the sides of C_2.

As a next step, alumo-carbons with a triatomic carbon core are considered. One point of interest here is whether or not analogous planar isomers can be found for larger systems. Another aspect is how a less-rigid core may be structurally affected by the considerable atom–atom interactions in the shell.

2.3.2.2 C_3Al_n ($n = 4$–8)

Thus, unlike C_2Au_n, not a single C_2Al_n ($n > 2$) isomer structurally resembles the corresponding C_2H_n. However, low-energy isomers of such alumo-carbons are still obtained when beginning with the hydrocarbon-like geometry, even though the structure alters considerably during optimisation. This is shown in particular for C_2Al_4, both discussed isomers of which are confirmed as the lowest and next-higher-energy structures in a direct extensive scan of the configuration space.[35] Stable systems with a larger tricarbon core can therefore be attempted to be produced also by relaxing their initial geometries similar to those of corresponding C_3H_n.

In particular, beginning with either propyne-like Al_2CCCAl_2 or propadiene-like $AlCCCAl_3$, the same relaxed structure of C_3Al_4 is obtained, with C_3 arching above the bent Al_4 rhombus (Figure 2.4). The longer tricarbon thus does not fit into the same frame as dicarbon in C_2Al_4, hence protruding from and distorting it. This structure can be viewed as a result of interaction between the originally linear C_3 molecule and the originally planar Al_4 cluster, or of addition of a 3rd C atom to the carbon core of rhombic C_2Al_4. It is worth noting that these possibilities thus appear to be, in effect, covered when using

hydrocarbon counterparts for initial geometries. An interesting feature is that in the corresponding anion the Al_4 base is shrunk and flat, the carbon core preserving its shape.

Beginning with propene-like $Al_2C{=}CAl\text{-}CAl_3$, the optimised structure of C_3Al_6 is a linear tricarbon in a symmetric hexagonal aluminium frame (Figure 2.4). Such a frame is thus large enough to accommodate the longer core in a planar geometry. Each outer atom of the core exhibits a planar tetra-coordination with bond angles close to 90°. The initially bent carbon core is thus straightened due to interaction with the aluminium component, exactly opposite to the shape variation for the above C_3Al_4 case.

Another isomer is produced from cyclopropane-like C_3Al_6. The carbon core becomes isosceles-triangular and is surrounded with an aluminium shell of a nonplanar (zigzagged) tetra-atomic frame plus one atom above and one under the core plane, so that the structure resembles Al_6 somewhat distorted by the C_3 cycle inside. This isomer is only ≈ 0.1 eV lower in energy relative to the above planar one, and each carbon atom is formally hexacoordinated. The strain in the core appears to be compensated by the more efficient bonding with the shell and in the shell itself.

Larger C_3Al_n systems can be obtained by adding more Al atoms to either of the above isomers of nearly the same energy. Adding more Al atoms to the planar C_3Al_6 isomer with the exposed carbon core and making new C–Al bonds could be expected to result in lower-energy systems as compared to just increasing the number of the (weaker) Al–Al interactions *via* adding Al atoms to the shell of the other C_3Al_6 isomer.

Two C_3Al_8 isomers are obtained by attaching Al_2 parallel to the face of planar C_3Al_6 and perpendicular to the carbon core (Figure 2.4). In one isomer the core angles away from and in the other one towards the added dimer positioned symmetrically or shifted to one end of the core, respectively. The symmetric isomer is ≈ 0.3 eV lower in energy and preserves an almost flat Al_6 frame. The other, skewed isomer can also be produced by relaxing structurally similar propane-like $Al_3C\text{–}CAl_2\text{–}CAl_3$ (with C_3 bent accordingly). Both or one, respectively, outer carbon atoms are formally hexacoordinated in these systems.

The equilibrium R_e(C–C) distance in C_3Al_n increases from $n = 4$ (≈ 1.3 Å) to $n = 6$ marginally (by ≈ 0.01 Å) for the planar isomer of C_3Al_6, the transition from a bent (at $\approx 150°$) to a linear core being compensated by more electron donors (Al atoms), or significantly (by ≈ 0.1–0.2 Å) for the nonplanar isomer, with the core bending further. Accordingly, for $n = 8$ (for more-stable isomer with C_3 bent at $\approx 130°$) the C–C distance increases as compared to planar, or decreases relative to nonplanar C_3Al_6 (with more strongly bent C_3). For the less-stable C_3Al_8 isomer, the core is bent less (by $\approx 150°$), the C–C distance being somewhat shorter.

The dissociation energy $D_e(C_3Al_n \rightarrow C_3 + n\ Al)$ per aluminium atom slightly decreases from ≈ 3.7 eV for $n = 4$ to ≈ 3.4 eV for $n = 6$, 8. The energy $D_e(C_3Al_n \rightarrow C_3Al_{n-2} + Al_2)$ for detachment of aluminium dimer, however, increases from ≈ 4.5 eV in C_3Al_6 to ≈ 5.5 eV in C_3Al_8. Somewhat counter-intuitively from the structural viewpoint and oppositely to the C_2Al_n case, the

energy $D_e(C_3Al_n \rightarrow C_3 + Al_n)$ for removal of the carbon core is smaller for $n = 6$ (≈ 7 eV) as compared to $n = 4$ (≈ 8.5 eV), likely due to a larger strain in planar C_3Al_6 as well as a larger structural relaxation of Al_6.

For C_3Al_4 to planar C_3Al_6 to more-stable C_3Al_8 the negative charge on the carbon core increases in absolute value linearly with the number of Al atoms, from -3.2e to -4.3e. The core charge is largest, at -4.5e, in the nonplanar isomer of C_3Al_6 and the less-stable isomer of C_3Al_8. Except in the nonplanar isomer of C_3Al_6, most of the charge is carried by the outer carbon atoms of the core, up to almost the neutral central atom in planar C_3Al_6. It is worth noting that in the anions extra charge is distributed mainly over the aluminium atoms (positive in the neutral system and thus attracting the extra electron). As a result, the Al atoms in, *e.g.*, $C_3Al_4^-$ become less charged and thus repel each other less, which explains the shrinking Al_4 base.

Dipole moments vary from zero for planar and small for nonplanar C_3Al_6 (≈ 0.5 D) to significant in C_3Al_4 and both isomer of C_3Al_8 (≈ 1–2 D). The vertical energies VE*, VIE, and VEA of C_3Al_n all peak (respectively at 3.2, 9.3, 1.5 eV) for $n = 4$ and have minimal values for $n = 6$.

The electron-density distribution indicates ionic bonding between the core and side Al atoms in C_3Al_4, while a weakly covalent bonding in planar C_3Al_6, with the C–Al critical electron densities equal for the axial and side atoms. The outer C atoms appear to make double bonds to the central C atom (not having bonds to the side Al atoms) and thus to formally have five bonds each, which could be facilitated by extra electrons on them (in terms of high negative charges). The AIM critical points indicate six bonds for one of the C atoms in nonplanar C_3Al_6 and for the outer atoms of the carbon core in symmetric C_3Al_8.

The small alumo-carbon clusters with a C_2 core thus exhibit structures very different from those of the corresponding auro-carbons. The fragmented gold shell with separate diatomic units is replaced with a more uniform aluminium shell, the latter tending to a 2D arrangement of atoms around the carbon core in case of its unsaturated bonding.

2.3.3 Larger Auro-Carbon Nanosystems

The above results clearly point to the carbon cores being able to shape the metal shells around them *via* a mixture of covalent and ionic bonding. So originally planar small gold clusters can be wrapped around carbon atom or diatom, as well as a carbon diatom and a triatom can stretch (without restructuring) or considerably restructure the small aluminium clusters (*e.g.* flattening them into 2D shells). In this section we will look at extensions to larger core–shell systems, and at the possibility for a carbon core to stretch a gold shell without a major restructuring of it.

2.3.3.1 $C_5Au_{12,14}$

Both CAu_4 and ethylene-like C_2Au_6 above (Section 2.3.1) exhibit stable structures with constituent methyl-like CAu_3 groups. From CAu_4 to this isomer

of C_2Au_6, one gold atom is replaced with such a group, similar to the structure evolution from methane to ethylene. If all four terminal H atoms of methane are replaced by CH_3 groups, neopentane (or tetramethylmethane) is formed. Upon a similar procedure with auro-carbon counterparts, a structurally analogous $C_5Au_{12} = C(CAu_3)_4$ system can be constructed.[36] The so-obtained gold shell around the carbon core correlates to a cuboctahedral isomer of the Au_{13} cluster with the central atom removed. We can also consider another, icosahedral-shaped Au_{13}, and use its different Au_{12} "surface" to accommodate the same C_5 core inside. The icosahedral shell can be seen as composed of four connected gold-atom triangles in a tetrahedral arrangement around its centre, to which four outer atoms of the carbon core can be bonded, again forming CAu_3 groups.

Relaxation of the above two structures only slightly distorts the original geometry of the gold shells, resulting in two isomers of C_5Au_{12}, icosahedral-like (I_h) and cuboctahedral-like (O_h), with the CAu_3 groups and the near-tetrahedral C_5 core preserved (Figure 2.5). The two isomers are nearly degenerate for the smaller basis set used, the O_h isomer becoming ≈ 0.5 eV lower in energy than the I_h one for the single-point calculation (in the frozen geometries) for the larger basis set.

The equilibrium C–C and C–Au distances of ≈ 1.6 and ≈ 2.1 Å are about same for both isomers, being exactly identical or varying within 0.05 Å for the I_h and O_h isomer, respectively. The Au–Au separations of around 3 Å are on average slightly longer for the I_h isomer, varying within 0.3 and 0.5 Å for the respective isomers. The C–Au and Au–Au distances in the CAu_3 groups are nearly the same as in C_2Au_6 calculated at the same level of theory.

The dissociation energy $D_e(C_5Au_{12} \rightarrow C_5 + 12\ Au)$ per gold atom, calculated relative to the lowest-energy (triplet) state of C_5 relaxed from its geometry of the core, is ≈ 1.5 eV. This is considerably lower than ≈ 2.4 eV for CAu_4 calculated at the same level of theory, reflecting a significant core relaxation,

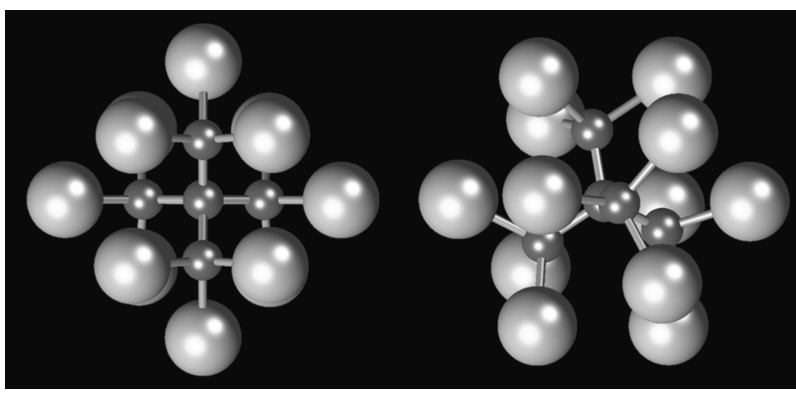

Figure 2.5 Optimised geometries of the O_h and I_h isomers of C_5Au_{12}.

hence its strain inside C_5Au_{12}. By comparison, relative to the frozen core this D_e value is ≈ 2.2 eV per gold atom.

For both isomers of C_5Au_{12}, the (natural) charge distribution is similar and shows a negative carbon core ($\approx -2.9 \pm 0.2$ e) and equally positive metal shell, qualitatively similar to the smaller systems considered above. In the core, the central C atom carries ≈ -0.3 e, about half the charge on each outer C atom.

Unlike the icosahedral Au_{12} shell that collapses if empty inside, the cuboctahedral cage isomer of Au_{12}, composed of three staggered square Au_4 units, is stable and has a closed-shell ground state, the triplet state being only ≈ 0.3 eV higher. It has the same dissociation energy of ≈ 1.5 eV per gold atom as the C_5Au_{12} system. Insertion of the carbon core thus reshapes (inflates) the gold shell mainly by stretching its central Au_4 square unit, while generally preserving the overall structure and stability. Hence, formation of this core–shell system relative to such a cage is approximately energy neutral, the shell inflation being compensated by the core–shell bonding.

Vertical ionisation energy (VIE) and electron affinity (VEA) of C_5Au_{12} are slightly lower (by 10–15%) relative to those of the Au_{12} cage (Table 2.3). The vertical spin-excitation energy VE*(S = 0 → 1), appreciable for the cage cluster, is, however, effectively cancelled in C_5Au_{12}.

We can approximately separate the dependences of the above properties on the gold shell geometry change only and the core–shell interaction *via* charge transfer, by calculating the property values for the shell frozen at the geometry in the total system. The $D_e(Au_{12} \rightarrow 12\ Au)$ is then ≈ 1.2 eV per atom, noticeably smaller due to stretched Au–Au distances and no core–shell Coulomb attraction. The ground state of the empty shell is actually triplet, though the singlet state is only slightly higher in energy (Table 2.3), similar to the situation for C_5Au_{12}, hence VE* is dominated by the shell shape. The VIE value for the empty shell is decreased relative to that for the gold cage by about a third of the total change, so the core–shell interaction is a major factor here. The VEA value significantly increases (by ≈ 1 eV or 30%) when the cage is inflated, but then decreases back when the core is inserted, to a value $\approx 10\%$ smaller than the original one. This suggests that both the geometry variation and the core–shell interaction affect this property about equally, but in opposite directions, effectively cancelling their contributions. Hence, different

Table 2.3 Characteristic energies (in eV) of the Au_{12} and XAu_{12} systems.

System	D_e[a]	*VE*(S = 0 → 1)*	*VIE*	*VEA*
Au_{13} (O_h isomer)	19.2	0.47[b]	6.90	3.45
Au_{12} cage (O_h isomer)	18.2	0.74	7.1	3.02
C_5Au_{12} (O_h isomer)	18.6	0.1[b]	6.18	2.68
Au_{12} in C_5Au_{12} (O_h), empty frozen shell	14.7	0.19[b]	6.78	3.96
$CH_4@Au_{12}$ ($\sim T_d$)	14.8	0.56	7.31	3.57
$H_2@Au_{12}$ (O_h)	16.5	0.45	7.2	3.40

[a] $Au_{12} \rightarrow 12$ Au, $XAu_{12} \rightarrow X + 12$ Au
[b] S = 1/2 → 3/2 for Au_{13}, S = 1 → 0 for C_5Au_{12} and Au_{12} shell

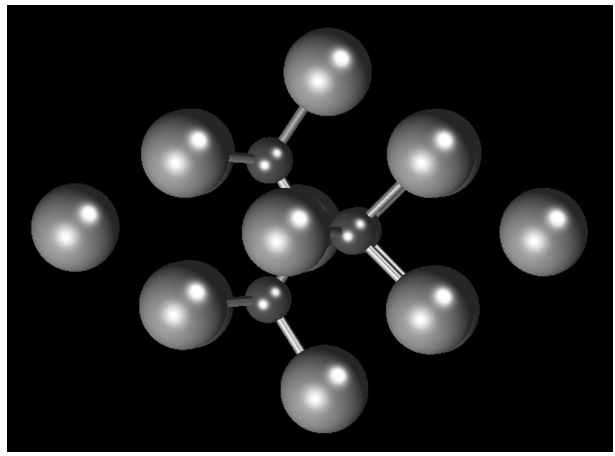

Figure 2.6 Optimised geometry of C_5Au_{14}.

properties exhibit very dissimilar evolutions when going from the Au_{12} cage to the C_5Au_{12} system.

The C_5Au_{12} system is structurally stable to adding more gold atoms. Its O_h isomer generally preserves shape when two Au atoms cap the smaller near-square Au_4 faces on opposite sides along the C_{2v} symmetry axis of the carbon core (Figure 2.6), becoming an elongated C_{2v}-symmetric C_5Au_{14} species. The stable C_5Au_{14} system exhibits a closed-shell singlet state marginally (by ≈ 0.1 eV) lower in energy than the triplet state, exactly opposite to C_5Au_{12} with its triplet ground state nearly degenerate with the singlet state. This could be related to the ''magic'' total number (34) of valence electrons in the atoms of C_5Au_{14}. Each of the two Au atoms in the formal 2nd shell around C_5 is bonded to C_5Au_{12} by ≈ 1.4 eV, *i.e.* only slightly less than the 1st shell atoms. The ionisation energy of ≈ 6.2 eV and electron affinity of ≈ 2.9 eV are nearly the same as for C_5Au_{12}.

2.3.3.2 $C_{10}Au_{18,21,24}$

Exploring further the structural analogy between the hydrocarbon and auro-carbon systems, the following larger-scale step is attempted. Formal removal of one methyl group of neopentane and dimerisation of the remainder *via* bonding two central C atoms produces a hexamethylethane molecule. A similar procedure for C_5Au_{12} would lead to a C_8Au_{18} counterpart that, however, is unstable, the central C–C bond dissociating upon relaxation.[37] This appears to be due to a strong repulsion between the closely spaced CAu_3 groups on different central carbon atoms. If an additional C_2 unit is introduced between those atoms, the two $C(CAu_3)_3$ components are spaced enough to prevent the dissociation of resulting $C_{10}Au_{18}$ (Figure 2.7), a counterpart of the di-t-butyl-acetylene hydrocarbon. The system thus has a C_3C–CC–CC_3 core surrounded by an

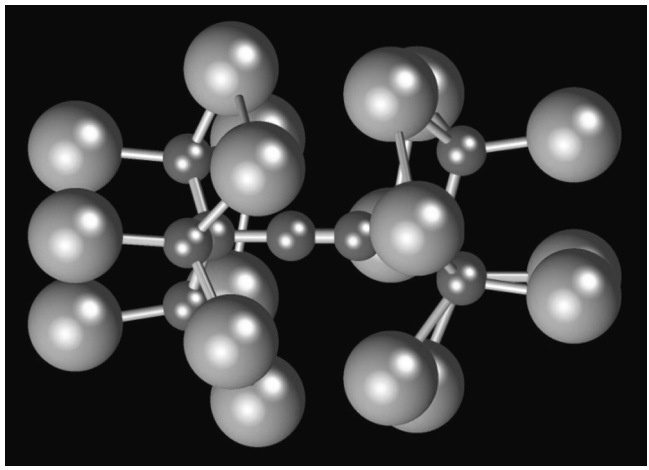

Figure 2.7 Optimised geometry of $C_{10}Au_{18}$.

ellipsoid-like Au_{18} shell composed of two staggered Au_6 rings and two triangular Au_3 caps.

Similar to C_5Au_{12}, the singlet and triplet states of $C_{10}Au_{18}$ are nearly degenerate within 0.05 eV. The ground state is closed-shell, different from the smaller system, likely due to the total of 58 valence electrons in all its atoms, which is another "magic" number, similar to the case of C_5Au_{14} *versus* C_5Au_{12} above.

In accordance with the bonding pattern, the C–C bond lengths increase from the centre (a triple bond), to the periphery of the core (single bonds of the sp–sp^3 and sp^3–sp^3 pairs of hybrids). The Au–Au equilibrium distances between two Au_6 rings are $\approx 3 \pm 0.1$ Å, the rings and caps being farther apart by ≈ 0.5 Å.

The dissociation energy $D_e(C_{10}Au_{18} \rightarrow C_{10} + 18\ Au)$ per gold atom is calculated for a relaxed C_{10} core in its lowest-energy triplet state, the value of ≈ 1.5 eV being the same as for the C_5Au_{12} counterpart. The $D_e(C_{10}Au_{18} \rightarrow C_{10}Au_{17} + Au)$ value of ≈ 1.8 eV is the same for detachment of a single gold atom from either ring or cap, in the latter case the detached atom being replaced by the ring atom, so the product is the same, with a missing ring atom.

Removal of the C_{10} core and relaxation results in a less-symmetric cage isomer of Au_{18} considerably (about twice) contracted along the former core axis and with distorted Au_6 rings, one ring becoming larger. The total dissociation energy of ≈ 1.7 eV per atom is somewhat higher than for $C_{10}Au_{18}$, reflecting the neutrality of and shorter Au–Au distances in the deflated cage. Insertion of the carbon core thus considerably symmetrises and inflates the gold shell *via* mainly stretching it along the core axis, while affecting stability relatively weakly.

The VIE and VEA values of $C_{10}Au_{18}$ are close to those of C_5Au_{12} (within 10%), the former being slightly lower (by ≈ 0.4 eV) and the latter slightly higher (by ≈ 0.2 eV). For the formal step-wise transition from the gold cage to the frozen empty gold shell to the shell with the carbon core inside, these vertical energies of the larger system evolve quite similarly to the case of the smaller

system. The only notable difference is the twice as large decrease of VIE (by ≈ 1.2 eV) when the core is inserted into the inflated shell.

The $C_{10}Au_{18}$ auro-carbon preserves its shape when another Au atom is attached to it. The resulting $C_{10}Au_{19}$ system is slightly more stable with the atom added to the side (between the rings) than to the cap (along the axis). The corresponding binding energies for this 2nd-shell atom are 2.3 ± 0.1 eV for the two isomers, which is larger than for C_5Au_{14} above. We can also anticipate a stable $C_{10}Au_{20}$ species with two capping atoms on the opposite sides along its axis.

The barrier for internal rotation of one $C(CAu_3)$ component of $C_{10}Au_{18}$ about the system axis is ≈ 0.3 eV, the associated transition state corresponding to the Au atoms of the two rings being opposite one another (*i.e.* aligned). This geometry can be stabilised by adding atoms into the 2nd gold shell, between the two rings. Attachment of three equally spaced Au atoms produces $C_{10}Au_{21}$, the added atoms occupying positions bridging two rather than capping four atoms in the two rings (Figure 2.8). As a result, the distance between the ring atoms slightly increases to ≈ 3.1 Å. The three atoms are bound by ≈ 2.5 eV per atom relative to relaxed $C_{10}Au_{18}$ (with staggered rings). Subsequent addition of capping Au atoms in the axial positions is expected to lead to stable $C_{10}Au_{22}$ and $C_{10}Au_{23}$ species.

Three more Au atoms added to the 2nd-shell ring around the original system can, however, have stable positions capping four ring atoms in resulting $C_{10}Au_{24}$ (Figure 2.9). The three gold pairs that are both capped and bridged stretch to ≈ 3.3 Å, and the binding energy of the 2nd-shell atoms to $C_{10}Au_{18}$ is then ≈ 2.0 eV per atom. A lower-energy isomer of $C_{10}Au_{24}$ has all six added atoms bridging pairs of opposite atoms in the rings and bound to original $C_{10}Au_{18}$ by ≈ 2.3 eV per atom. One and two capping gold atoms added along the system axis are anticipated to result in stable $C_{10}Au_{25}$ and $C_{10}Au_{26}$.

The charge distribution in $C_{10}Au_{18}$ exhibits a carbon core that is increasingly negative from its (nearly neutral) centre to periphery, and relatively uniformly positive gold shell having most of positive charge in the middle (on the rings). The system thus has a significant quadruple moment whose electric field can significantly polarize the 2^{nd}-shell gold atoms in larger systems, consistent with the above higher binding energies of the added atoms to $C_{10}Au_{18}$. By comparison, in C_5Au_{12} the more centrally symmetric charge distribution can result in a much weaker electric field, with the core and shell fields effectively cancelling each other. Furthermore, the total charge on the C_{10} core is ≈ -4.0 e, significantly larger than on the C_5 core, in accordance with the number of the Au donors in the shell.

So far pure-carbon radical cores are considered, forming bonds to the shell atoms. In the next section, the core is represented by a closed-shell molecule interacting with the metal atom shell noncovalently.

2.3.4 A Gold Cage Structured by a Hydrocarbon Molecular "Dopant"

Another, qualitatively different structural modification of the C_5 radical core is replacement of its outer carbon atoms by hydrogens, leading to a closed-shell

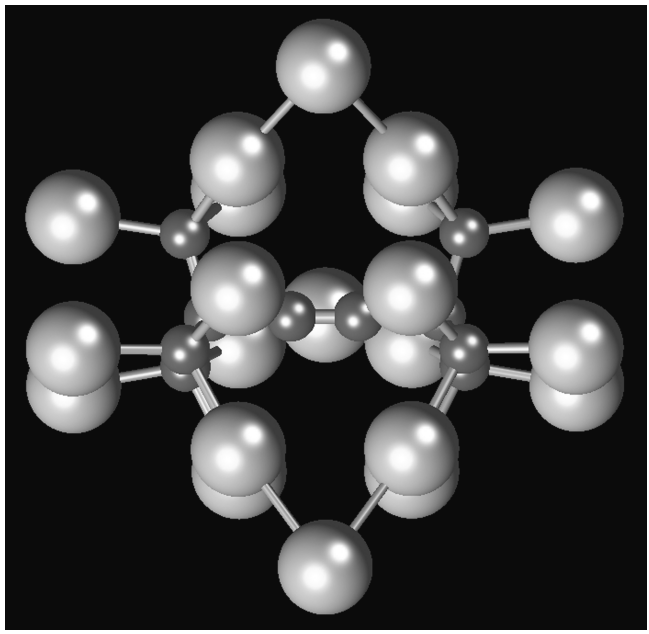

Figure 2.8 Optimised geometry of $C_{10}Au_{21}$.

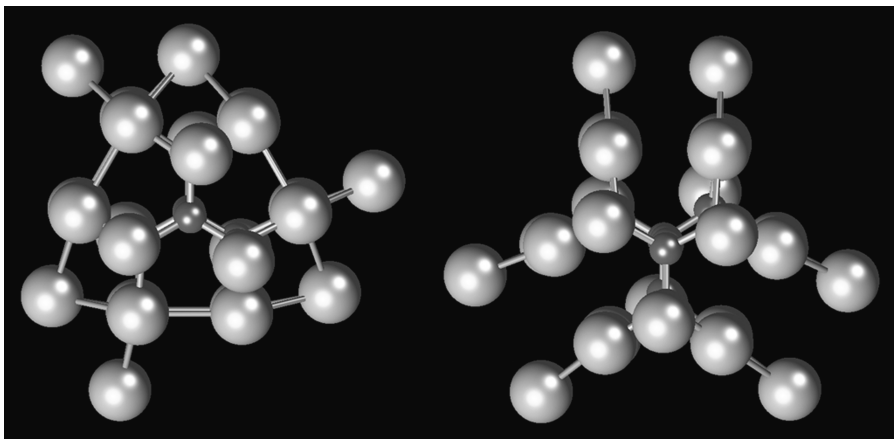

Figure 2.9 Optimised geometries of the isomers of $C_{10}Au_{24}$.

counterpart, tetrahedral methane molecule CH_4. When inserted inside Au_{12} in place of C_5, such a core can either break the gold shell (starting with the O_h isomer of C_5Au_{12}) or transform it considerably (using the I_h isomer as a starting point). In the latter case the molecule is then suspended centrally inside its truncated-tetrahedral-like frame with no bonds formed (Figure 2.10). The

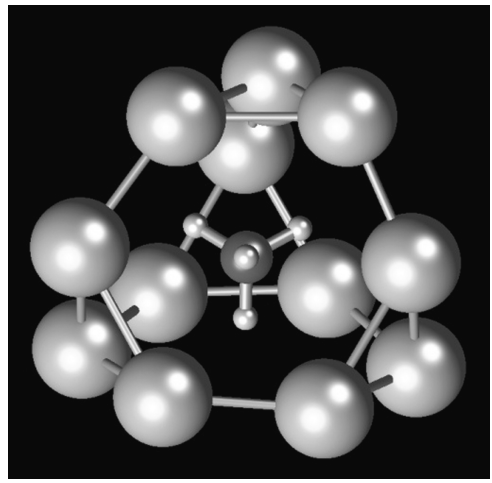

Figure 2.10 Optimised geometry of $CH_4@Au_{12}$.

H-ends of the molecule appear to make large hexagonal holes in the shell composed of four triangular units bonded by their corners.

All equilibrium C–Au and Au–Au distances are $\approx 3.3 \pm 0.2$ and ≈ 2.8–2.9 Å, respectively, indicating a larger overall size of the gold shell, while on average slightly shorter Au–Au distances as compared to C_5Au_{12}. Each C–H bond points to the centre of Au_6 (nonflat) "facet", each Au_3 "facet" being at the hollow of the methyl side of CH_4, in a staggered arrangement with hydrogen atoms. For the rotated-core geometry with the H ends pointing into the centres of the Au_3 "facets" the energy is ≈ 1.2 eV higher and upon relaxation the system recovers the original geometry. It is also recovered if the molecule is shifted from the centre of the cage by up to as much as ≈ 1 Å, clearly suggesting the obtained geometry as an isomer of the system.

The gold shell collapses if the molecular core is removed. The energy barrier to such a removal by pulling CH_4 through the hexagonal hole is evaluated to be ≈ 2 eV. The $D_e(CH_4@Au_{12} \rightarrow CH_4 + 12\ Au)$ dissociation energy is ≈ 1.2 eV per atom, which is somewhat less than for C_5Au_{12}, reflecting no bonding between the core and the shell. For the frozen Au_{12} shell with no core inside, the total dissociation energy is ≈ 0.1 eV per atom higher, indicating a slightly repulsive core–shell interaction in $CH_4@Au_{12}$, the molecule thus inflating the cage. This is supported by the C–Au distances (for the central C atom) being slightly longer than in C_5Au_{12}.

Unlike the molecular radical (C_5), the similarly shaped molecule (CH_4) thus changes the gold shell structure considerably. This can be associated with noncovalent interaction between the closed-shell core and the shell, different from the core–shell bonding in C_5Au_{12} and thus leading to a different match of the core and shell geometries. In addition, the methane core remains essentially neutral, different from the extensive core–shell charge transfer for the other case.

The closed-shell $CH_4@Au_{12}$ system exhibits a significant singlet–triplet vertical gap VE* (Table 2.3), different from the near-degenerate case of C_5Au_{12}. For the methane-based system the VIE value is $\approx$20% higher and the VEA value $\approx$30% eV higher, consistent and counter intuitive, respectively, with the closed-shell nature of the CH_4 "dopant".

Because of noncovalent interactions between methane and the gold cage, limited test calculations have been carried out at the MP2 level as well. The above geometry of the system is confirmed, and its stability to dissociation into the separate molecule and gold atoms increases by 25% relative to the DFT result.

Hence, CH_4 is a molecule barely fitting into the Au_{12} shell. Moreover, it appears to break the cuboctahedral gold cage (stable by itself) when inserted there. Therefore, next, we consider a smaller (actually the smallest possible) molecule to see if it could fit into such a cage without breaking it.

2.3.5 Hydrogen Trapping in Metal Cluster Nanocages

2.3.5.1 $H_2@Au_{12}$

If H_2 is inserted into the icosahedral-like Au_{12} cluster cage (instead of C_5 in the I_h isomer of C_5Au_{12} above), the cage breaks, unlike for the CH_4 "dopant" above. However, the other, cuboctahedral cage survives the intrusion, and two nearly degenerate isomers of the resulting $H_2@Au_{12}$ system are found, with the molecule oriented approximately along and perpendicular to the cage axis (Figure 2.11). In the latter case, the molecule is aligned with two diagonal atoms of the central square unit of the gold cage. For both isomers, this central square of the cage (directly around the molecule) is stretched by $\approx$0.5 Å in the Au–Au distance, while the H_2 molecule is essentially intact and neutral.

The ground state of the system is closed-shell, the triplet state being only $\approx$0.1 eV higher in energy. The $D_e(H_2@Au_{12} \rightarrow H_2 + 12\ Au)$ dissociation energy of $\approx$1.4 eV per gold atom ($\approx$0.1 eV per atom smaller than for the relaxed cage) is consistent with some inflation of the cage by the core. The smaller such value found for $CH_4@Au_{12}$ above is in accordance with a larger inflation of the cage by the larger core. The energy of $H_2@Au_{12}$ being higher (by $\approx$1.7 eV) than separate H_2 and Au_{12} cage implies metastability of the core-shell structure.

The VIE and VEA values remain almost unchanged or slightly increase (within 15%) relative to those of the Au_{12} cage (Table 2.3). The VE*($S = 0 \rightarrow 1$) value shows a more pronounced relative decrease (by $\approx$40%), remaining small (under 1 eV).

Test MP2 calculations confirm geometries and near-degeneracy of the two isomers of $H_2@Au_{12}$. The system stabilisation relative to separate gold atoms and the molecule is increased by $\approx$40% as compared to the DFT data. This is a larger difference than for the $CH_4@Au_{12}$ above, in accordance with a denser packing of gold atoms in $H_2@Au_{12}$ and an underestimation of the aurophilic interaction by DFT (predicting, for instance, weakly repulsive Au–Au

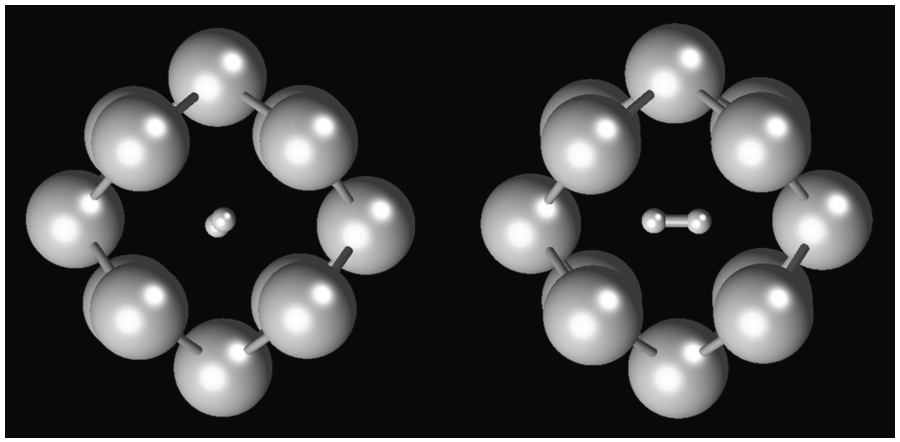

Figure 2.11 Optimised geometries of the isomers of $H_2@Au_{12}$.

interactions in CAu_4 using the same model as in Section 2.3.1.1 above). The system is also confirmed to be metastable relative to $H_2 + Au_{12}$ by $\approx 2\,eV$.

Thus, hydrogen molecules can be accommodated inside a small gold cage, inflating but not distorting it dramatically. For comparison, let us also consider hydrogen inside a cluster cage made of another metal.

2.3.5.2 $H_2@Mg_{8,9,10}$ and $(H_2)_2@Mg_{10}$

Bulk magnesium hydrate, MgH_2, is a promising material for hydrogen storage. It is structurally built of linear HMgH units resembling isolated molecules of such atomic composition. One difficulty with a practical use of this material is the need to break Mg–H bonds to withdraw hydrogen, which requires high temperatures. However, there is another, weakly bound $Mg–H_2$ isomer of the same molecule, of nearly same energy (with two Mg–H bonds replaced by a strong H–H bond). Removal of hydrogen from such a complex can be expected to be easy due to no bond-breaking, or even oppositely, a low temperature may be needed to prevent dissociation of this complex. Structural extensions of the system, capable to trap H_2 more reliably, are Mg_nH_2 clusters. Since a more practical storage requires a higher hydrogen-to-magnesium weight ratio, the smallest clusters are considered.[38]

Appropriate cage structures are known for small Mg_n, including those with $n = 5$ and 7 (trigonal and pentagonal bipyramids), and 9 (tricapped trigonal prism). Attempts to insert hydrogen molecules into Mg_5 and Mg_7 fail, the cages breaking due to being too tight to accommodate the molecule. The Mg_9 cage is the first survivor, with its structure reshaping from three staggered triangles in Mg_9 to two staggered squares capped on one side in $H_2@Mg_9$, all nearest-neighbour Mg–Mg distances being ≈ 3 Å. The H_2 molecule is oriented axially

and shifted away from the capping atom (Figure 2.12), while being considerably stretched (by ≈ 0.2 Å) relative to the isolated diatom.

Detachment of capping Mg results in a more symmetric $H_2@Mg_8$ system, with the molecular hydrogen core located centrally inside the magnesium shell of two staggered Mg_4 squares. These squares are slightly larger (by ≈ 0.1 Å in side) and further apart than in $H_2@Mg_9$, while H_2 is stretched less, by ≈ 0.1 Å. The cage geometry is significantly different from that of the isolated Mg_8 cluster (capped pentagonal bipyramid) and is also obtained upon inserting H_2 into its centre and relaxing the system.

Alternatively, attachment of another capping atom to the opposite side of the Mg_9 cage stretches the molecule further and, it turns out, beyond its breaking point. The resulting $H_2@Mg_{10}$ system is represented by two H atoms ≈ 2 Å apart (approximately at the centres of the Mg_4 squares), encapsulated in the Mg_{10} shell of two square pyramids joined by their (staggered) bases, all Mg–Mg distances being slightly shorter (by ≈ 0.05 Å) than in $H_2@Mg_9$. The cage structure differs considerably from that of isolated Mg_{10} (capped trigonal prism

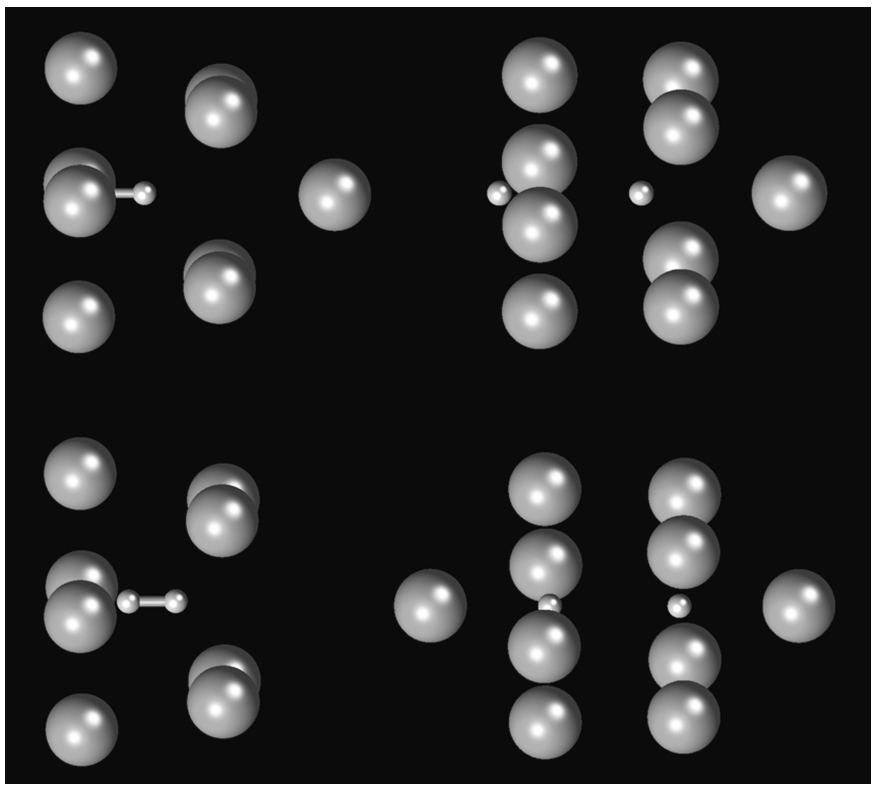

Figure 2.12 Optimised geometries of the isomers of $H_2@Mg_9$ with non- and dissociated H_2 (top row), $H_2@Mg_8$ and $H_2@Mg_{10}$ (bottom row).

that is recovered if H_2 is removed) and is produced also when H_2 is inserted into it.

Uncapping $H_2@Mg_{10}$ does not recover the above $H_2@Mg_9$ structure with nondissociated H_2 but produces another, dissociated-core isomer of the system with two H atoms even slightly further apart (by ≈ 0.1 Å) and shifted axially further away from the other capping atom. The cage slightly shrinks in general as compared to $H_2@Mg_{10}$, and the system is ≈ 0.1 eV lower in energy than the first isomer of $H_2@Mg_9$. The energy barrier between these isomers, *i.e.* for dissociation of hydrogen inside the Mg_9 cage, is ≈ 0.1 eV only. In accordance with the above, this barrier vanishes when $H_2@Mg_9$ is axially capped by another Mg atom.

The evolution of the hydrogen core with the number of atoms in the magnesium shell can be associated with the core–shell charge transfer. With increasing number of Mg atoms, more and more electron density is transferred to H_2, leading to its stretch and finally dissociation. Starting from ≈ -0.3 e on the molecule for $n = 8$, the charge more than doubles (to ≈ -0.8 e on nondissociated H_2) for $n = 9$, and reaches ≈ -1 e on each H atom for $n = 10$, thus in fact leading to a Coulomb explosion of the core, induced by and confined in the shell. Accordingly, the Coulomb attractions contract the increasingly positive cage around the molecule, which explains the above shrinking of the magnesium shell from $n = 8$ to 10. The axial Mg atoms are charged more than the side ones.

The $D_e(H_2@Mg_n \rightarrow H_2 + n\,Mg)$ dissociation energy increases about linearly with n, from ≈ 3 eV for $n = 8$ to ≈ 7 eV for $n = 10$, indicating a detachment energy of ≈ 2 eV per capping atom and considerably smaller values for the Mg_4 squares (≈ 0.4 eV per atom for $n = 8$), consistent with their relative charges. The energy $D_e(H_2@Mg_n \rightarrow H_2 + Mg_n)$ for the molecule withdrawal from the cluster cage is slightly negative, varying from ≈ -0.3 eV to ≈ -0.1 eV to ≈ -0.8 eV for $n = 8$ to 10. The $H_2@Mg_9$ system being thus relatively most stable is formally consistent with the "magic" total number (20) of valence electrons in its atoms. Pressing two H anions closer to each other inside the Mg_{10} shell as compared to the Mg_9 case reduces the system stability. The resulting slight metastability of $H_2@Mg_n$ can be considered as a positive factor in facilitating hydrogen release when needed.

All the above $H_2@Mg_n$ are closed shell systems, similar to $H_2@Au_{12}$. Unlike for the former system, however, the molecule does not dissociate inside the gold cage and remains essentially neutral, similar to the above $CH_4@Au_{12}$ case and different from the case of a magnesium cage. For both metals, the cages with trapped H_2 are metastable, more so for the case of the gold shell exhibiting no significant charge transfer to the core, in accordance with a higher electronegativity of Au as compared to Mg.

An interesting feature of the $H_2@Mg_n$ systems is their slightly negative or near-zero VEA values, varying from ≈ -0.2 eV for $n = 8$ to ≈ 0.1 eV for $n = 10$. This, together with their appreciable VIE and VE* values (≈ 6 to ≈ 7 eV and ≈ 1 to ≈ 3 eV, respectively), would make these species rather nonreactive and thus observable when formed in experiments.

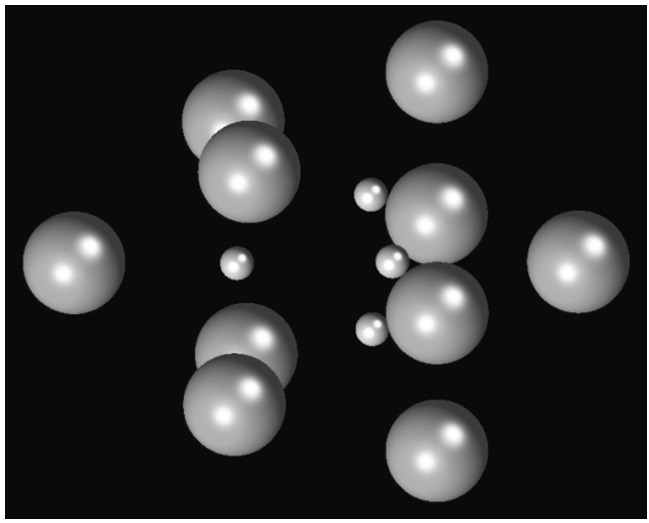

Figure 2.13 Optimised geometry of $(H_2)_2@Mg_{10}$.

Following the above dissociation of H_2 inside Mg_{10}, another cage catalysed and confined reaction can be simulated. Two H_2 molecules are initially placed axially inside the same cage near centres of two Mg_4 squares, and the system is relaxed. Both molecules dissociate and the system goes through a transition state with a newly formed H_2 molecule at the centre and two H atoms symmetrically on its sides, all still lying along the system axis. Then, the central molecule shifts away from the axis and finally merges with one of side H atoms into a symmetric H_3 species with the H–H separation of ≈ 1.1 Å and bent (at $\approx 150^\circ$) "around" the other H atom remaining in the axis ≈ 2 Å away from each atom of H_3 (Figure 2.13). The cage adjusts as well, by stretching the Mg_4 unit around H_3 from a square to a rectangle.

Here, we thus see an example of a magnesium-cage induced reaction that can be written as $(H_2 + H_2 \rightarrow 2H + H_2 \rightarrow H + H_3)@Mg_{10}$. The product system is ≈ 1 eV lower in energy than the above transition state and is metastable by ≈ 1 eV relative to $2H_2 + Mg_{10}$. The reaction is again of a charge-transfer-induced type, with the hydrogen component being negative during the process and represented by $H^{-0.2} + {H_3}^{-2.2}$ in the end.

2.4 Conclusions

A series of cluster systems of mixed metal–nonmetal composition is considered from the viewpoint of designing stable core–shell systems. The core varies in size from a single atom (C) to a diatom (C_2, H_2) to a larger molecular species (CH_4, $(H_2)_2$, $C_{3,5,10}$), and the shell is constructed of metal atoms (Au, Al, Mg) starting from a few and up to 24.

The gradual increase of the number of gold atoms in small CAu_n clusters indicates a 2D to 3D transition at $n = 4$, much earlier than for pure Au_n (around $n = 13$, ref. 14). The carbon atom is then positioned at the centre of a tetrahedral, square-pyramidal and octahedral shaped layer of gold atoms for $n = 4$ to 6, respectively, for the lowest-energy isomers. Other isomers correspond to different shell shapes, and/or noncentral up to (higher-energy) surface locations of the C atom. Up to $n = 4$, CAu_n are structural analogues of CH_n.

The gold shells around the dicarbon core include diatomic units (in accordance with closed-shell Au_2), at least for the lowest-energy isomers of small C_2Au_n, reflecting interplay between C–Au and Au–Au bonding. The most stable geometries for $n > 2$ resemble those of weakly bound hydrocarbon complexes (hydrogen–acetylene, *etc.*), while the structural counterparts of hydrocarbon molecules, dominated by C–Au bonding, are the lowest-energy isomer for $n = 2$ or the isomers of slightly higher energy for $n \geq 3$.

By comparison, small C_2Al_n (and C_3Al_n) clusters, consistent with higher valence offering more options for Al–Al bonding and with open-shell Al_2, are different and do not exhibit diatomic units as well as (except for $n = 2$) stable hydrocarbon-like structures that in fact may correspond to transition states. In particular, unsaturated alumocarbons (C_2Al_4, C_3Al_6) tend to have lowest- or at least low-energy planar geometries with aluminium 2D shells (frames) around linear carbon cores. The cores can bend and protrude from the frames in the case of their size mismatch (as for C_3Al_4) or in saturated systems (C_3Al_8).

The structural similarity of the low-energy isomers of the small auro-carbon species to analogous hydrocarbons enables starting with appropriate C_nH_m counterparts to build larger core–shell auro-carbons, such as C_5Au_{12} and $C_{10}Au_{18}$. The aurophilic interactions allow further design options employed in extending and realigning the shells in C_5Au_{14} and $C_{10}Au_{21,24}$, with an apparent feasibility of other similar species. In particular, the usually increased stability of systems with "magic" number of valence electrons (like 8 in CAu_4, 34 in C_5Au_{14}, 58 in $C_{10}Au_{18}$) can be another factor to account for in design. Due to an appreciable difference in relative electronegativities of carbon and metals, however, this factor may be of limited validity. For instance, while CAu_4 is the most stable of small CAu_n systems in terms of dissociation and shows a considerable singlet-triplet gap, the larger C_5Au_{14} and $C_{10}Au_{18}$ systems have the closed-shell ground state only marginally lower in energy than the excited open-shell state. In the case of still less electronegative Al, formally "magic" C_2Al_4 is actually least stable among its size-neighbours in either core or shell.

The switch from unsaturated molecules and molecular radicals (such as C_n) to closed-shell molecules like CH_4 and H_2 adds more variety to the core–shell system geometries and related properties due to different (noncovalent) interactions between the core and the shell. In particular, the geometrically C_5-like methane core completely restructures the gold shell as compared to that in C_5Au_{12}, while molecular hydrogen only slightly inflates the cuboctahedral Au_{12} cage and appears to be able to rotate inside it relatively freely. This can allow creation of species with unique geometries and parameters. Due to no core–shell bonding and charge transfer (unlike in C_nAu_m), these systems are

metastable (higher in energy) relative to the molecules being outside the shells. Some of the shells (*e.g.* that in $CH_4@Au_{12}$) may collapse with no supporting cores inside, while some cages stable by themselves (like cuboctahedral Au_{12}) may break upon insertion of such a core (*e.g.* CH_4), so there is a composition-specific balance to be found in designing such species.

Some other, sufficiently tight, metal cages, such as Mg_{8-10}, can be significantly reshaped by insertion of even the smallest possible, H_2, molecule. Such systems with shells of less electronegative metal atoms can exhibit a significant core–shell charge transfer. This may result in induced dissociation of the core, and in more complicated chemical reactions between components of a core composed of a few molecules, steered in the confined spaces of and catalysed by the surrounding metal shell, as illustrated by $(2H_2)@Mg_{10}$.

Manifestation of structure–property relationships can be noted in terms of comparing vertical excitation and ionisation energies (VE*, VIE) and electron affinities (VEA) of the empty metal cluster cage and the corresponding core–shell system. For instance, these properties may be affected relatively weakly, as in CAu_5 as compared to Au_5, or vary differently and more strongly, as for other CAu_n, in particular in opposite directions for different n, as for $n = 4$ and 6. Similarly, the properties of a stable empty cage may be altered only slightly by insertion of a small molecule, as for $H_2@Au_{12}$, or more significantly, as in C_5Au_{12}. The properties may also vary in different directions for different molecular cores, such as VEA for $H_2@Au_{12}$ *versus* C_5Au_{12}. Such a variety of possible property modifications makes it possible to selectively design and fine tune desirable parameters of core–shell systems by combining proper cores and shells.

Possible applications of such core–shell systems may include tunable catalysts, molecular (including hydrogen) storage, molecular electronics, nanostructures and nanomaterials, *etc*. In particular, the metastability of species such as H_2 trapped in a metal cage could enable relatively easy release of hydrogen when needed. Moreover, such a metastability can also be considered as energy storage at the molecular/cluster level, providing, in the case of hydrogen, an additional, direct component of accumulated energy.

Acknowledgements

The author is grateful to P. McNelles and G. Kochhar for preliminary calculations on some of the above systems during their 4th-year thesis and Summer research. Acknowledged with gratitude are the financial support of the UOIT and NSERC of Canada, and the technical support of the staff of high-performance computing facilities of the UOIT Faculty of Science and of the SHARCnet distributed academic network of Ontario.

References

1. J. A. Alonso, *Chem. Rev.*, 2000, **100**, 637.
2. E. Roduner, *Chem. Soc. Rev.*, 2006, **35**, 583.

3. M. C. Daniel and D. Astruc, *Chem. Rev.*, 2004, **104**, 293.
4. D. E. Bergeron, A. W. Castleman Jr., T. Morisato and S. N. Khanna, *Science*, 2004, **304**, 84.
5. O. P. Charkin, D. O Charkin, N. M. Klimenko and A. M. Mebel, *Chem. Phys. Lett.*, 2002, **365**, 494.
6. C. Majumder, A. K. Kandalam and P. Jena, *Phys. Rev. B*, 2006, **74**, 205437.
7. V. Kumar, *Comput. Mater. Sci.*, 2006, **36**, 1.
8. M.-M. Rohmer, M. Bénard and J.-M. Poblet, *Chem. Rev.*, 2000, **100**, 495.
9. R. Ferrando, J. Jellinek and R. L. Johnston, *Chem. Rev.*, 2008, **108**, 845.
10. M. P. Johansson, D. Sundholm and J. Vaara, *Angew. Chem. Int. Ed.*, 2004, **43**, 2678.
11. W. Fa and J. Dong, *J. Chem. Phys.*, 2006, **124**, 114310.
12. R. J. C. Batista, M. S. C. Mazzoni, L. O. Ladeira and H. Chacham, *Phys. Rev. B*, 2005, **72**, 085447.
13. C. Chang, A. B. C. Patzer, E. Sedlmayr, D. Sülzle and T. Steinke, *Comput. Mater. Sci.*, 2006, **35**, 387.
14. W. Fa, C. Luo and J. Dong, *Phys. Rev. B*, 2005, **72**, 205428.
15. D. Y. Zubarev and A. I. Boldyrev, *J. Chem. Phys.*, 2005, **122**, 144322.
16. R. Pal, S. Bulusu and X. C. Zeng, *J. Comput. Meth. Sci. Eng.*, 2007, **7**, 185.
17. B. Kiran, H.-J. Zhai, L.-F. Cui and L.-S. Wang, *Angew. Chem. Int. Ed.*, 2004, **43**, 2125.
18. M. Lahav, E. A. Weiss, Q. Xu and G. M. Whitesides, *Nanolett.*, 2006, **6**, 2166.
19. E. J. Bylaska, W. A. de Jong, K. Kowalski, T. P. Straatsma, M. Valiev, D. Wang, E. Aprà, T. L. Windus, S. Hirata, M. T. Hackler, Y. Zhao, P.-D. Fan, R. J. Harrison, M. Dupuis, D. M. A. Smith, J. Nieplocha, V. Tipparaju, M. Krishnan, A. A. Auer, M. Nooijen, E. Brown, G. Cisneros, G. I. Fann, H. Fruchtl, J. Garza, K. Hirao, R. Kendall, J. A. Nichols, K. Tsemekhman, K. Wolinski, J. Anchell, D. Bernholdt, P. Borowski, T. Clark, D. Clerc, H. Dachsel, M. Deegan, K. Dyall, D. Elwood, E. Glendening, M. Gutowski, A. Hess, J. Jaffe, B. Johnson, J. Ju, R. Kobayashi, R. Kutteh, Z. Lin, R. Littlefield, X. Long, B. Meng, T. Nakajima, S. Niu, L. Pollack, M. Rosing, G. Sandrone, M. Stave, H. Taylor, G. Thomas, J. van Lenthe, A. Wong, Z. Zhang, *NWChem, A Computational Chemistry Package for Parallel Computers*, Version 5.0, Pacific Northwest National Laboratory, Richland, Washington 99352-0999 (USA), 2006.
20. A. Ryzhkov and A. Antipin, *ViewMol3D 4.34, a 3D OpenGL viewer for molecular structures.* http://redandr.tripod.com/vm3/
21. *Basis Set Exchange*, v. 1.2.2, Pacific Northwest National Laboratory, Richland, Washington 99352-0999 (USA). https://bse.pnl.gov/bse/portal
22. *NIST Chemistry WebBook* (NIST Standard ref. Database Number 69, June 2005 Release). http://webbook.nist.gov/chemistry/
23. M. Walter and H. Häkkinen, *Phys. Chem. Chem. Phys.*, 2006, **8**, 5407.
24. Q. Sun, Q. Wang, G. Chen and P. Jena, *J. Chem. Phys.*, 2007, **127**, 214706.

25. B. W. Ticknor, B. Bandyopadhyay and M. A. Duncan, *J. Phys. Chem. A*, 2008, **112**, 12355.
26. C. Majumder, *Phys. Rev. B*, 2007, **75**, 235409.
27. W. Zhizhong, Z. Xiange and T. Auchin, *J. Mol. Struct. (Theochem)*, 1998, **453**, 225.
28. P. Zaleski-Ejgierd and P. Pyykko, *Can. J. Chem.*, 2009, **87**, 798.
29. K. Chenoweth and C. E. Dykstra, *Chem. Phys. Lett.*, 2004, **153**, 400.
30. F. Y. Naumkin, *J. Phys. Chem. A*, 2008, **112**, 4660.
31. A. I. Boldyrev, J. Simons, X. Li, W. Chen and L.-S. Wang, *J. Chem. Phys.*, 1999, **110**, 8980.
32. N. A. Cannon, A. I. Boldyrev, X. Li and L.-S. Wang, *J. Chem. Phys.*, 2000, **113**, 2671.
33. X. Li, L.-S. Wang, N. A. Cannon and A. I. Boldyrev, *J. Chem. Phys.*, 2002, **116**, 1330.
34. R. F. W. Bader, *Atoms in Molecules: A Quantum Theory*, Oxford University Press, Oxford, 1990.
35. Y.-B. Wu, H.-G. Lu, S.-D. Li and Z.-X. Wang, *J. Phys. Chem. A*, 2009, **113**, 3395.
36. F. Naumkin, *Phys. Chem. Chem. Phys.*, 2006, **8**, 2539.
37. F. Y. Naumkin, *Chem. Phys. Lett.*, 2008, **466**, 44.
38. P. McNelles and F. Y. Naumkin, *Phys. Chem. Chem. Phys.*, 2009, **11**, 2858.